FFI-RAPPORT

20/00616

Testing a simple velocity fluctuation model for one-dimensional simulations of shock-wave particle cloud interaction

Bernhard Nornes Lotsberg
Andreas Nygård Osnes

Testing a simple velocity fluctuation model for one-dimensional simulations of shock-wave particle cloud interaction

Bernhard Nornes Lotsberg
Andreas Nygård Osnes

Norwegian Defence Research Establishment (FFI) 17 June 2020

Keywords
Computational Fluid Dynamics (CFD)
Flerfasestrømning
Turbulent strømning
Sjokkbølger

FFI report
20/00616

Project number
1393

Electronic ISBN
978-82-464-3277-9

Approvers
Anders Helgeland, *Research Manager*
Janet Martha Blatny, *Research Director*

The document is electronically approved and therefore has no handwritten signature.

Summary

Airborne dispersal of toxic substancres in populated regions is a central research topic at the Norwegian Defence Research Establishment (FFI). Such an event can be the result of accidents in industrial areas or during transport. Acts of terrorism are also a possible source of such releases. The ability to model airborne dispersion with sufficient accuracy makes it possible to characterize the threath such events pose. Such modelling can also be used to be better prepared and respond appropriately to an event. This report is a part of a research project that aims to improve models for simulation of dispersal of toxic substances by means of explosive devices. Specifically, this work is part of a research effort to improve models for computing the movement of solid particles under shock-wave acceleration.

The purpose of this study is to test a model for velocity fluctuation correlations caused by particle wakes in simulations of shock particle-cloud interactions. Velocity fluctuations are dynamically important in such flows, and accurate models for their correlations are therefore necessary. Improved models for shock wave particle-cloud interaction enable more accurate simulations of various important applications such as shock wave mitigation, explosive dissemination of powders and liquids, heterogeneous explosives and liquid/solid fuel combustion systems.

In this work, we have implemented the velocity fluctuation model in an in-house finite-volume Eulerian-Lagrangian compressible flow solver, which is based on the volume-averaged Navier-Stokes equations. The model can be expressed

$$\tilde{R} \approx \tilde{u}^2 \frac{C_{\text{sep}}\alpha_{\text{p}}}{\alpha - C_{\text{sep}}\alpha_{\text{p}}},$$

where $\tilde{R}$ is the velocity fluctuation correlation, $\tilde{u}$ is the mean flow velocity, and $\alpha_{\text{p}} = 1 - \alpha$, where α is the gas volume fraction. The model has one parameter, C_{sep}, which we estimate using the ABC-SMC algorithm based on results from a particle-resolved simulation of the same system. Application of the ABC-SMC algorithm for parameter estimation is an interesting approach since the estimated value is optimal for the specific implementation of the dispersed flow model.

Depending on whether we use an approximate drag law or the actual forces from the particle-resolved simulations, the parameter is estimated to $C_{\text{sep}} = 1.4$ and $C_{\text{sep}} = 1.6$ respectively. The physical meaning of these values is that the average volume of the separated flow behind each particle is 1.4 or 1.6 times larger than the particle volume. The dependence of the estimated parameter value to the choice of drag law implies that to get a physically meaningful value for C_{sep}, we need to use a drag law that accurately represents both the transient and quasi-steady forces on the particles.

Sammendrag

Luftbåren spredning av trusselstoffer i områder der det befinner seg mennesker er en sentral problemstilling hos Forsvarets Forskningsinstitutt (FFI). En slik hendelse kan for eksempel være et resultat av ulykker i industriområder eller ved transport. Terrorhandlinger er også en mulig kilde til slike utslipp. Dersom man kan modellere luftbåren spredning med tilstrekkelig nøyaktighet vil man være i stand til å karakterisere trusselen slike hendelser utgjør, og man vil være i bedre stand til forberede seg, samt respondere på en hensiktsmessig måte, på en hendelse. Denne rapporten er en del av et arbeid for å utvikle bedre metoder for å beregne spredning av trusselstoffer fra eksplosive kilder. Spesifikt er denne studien en del av et prosjekt som har som mål å forbedre modeller for å beregne bevegelsen til faste partikler når de blir aksellerert av en sjokkbølge.

Målet med denne studien er å teste en modell for korellasjon av hastighetsfluktuasjoner skapt av partikkelvaker i simuleringer av sjokk-partikkelsky interaksjon. Hastighetsfluktuasjoner er viktige for dynamikken i slike strømninger, og det er derfor nødvendig å ha nøyaktige modeller for korrelasjonene deres. Forbedrede modeller for sjokk-partikkelsky interaksjon muliggjør nøyaktige beregninger av forskjellige viktige anvendelser, for eksempel demping av sjokkbølger, eksplosiv spredning av pulver og væsker, heterogene eksplosiver og forbrenningssystemer med både fast og flytende drivstoff.

I dette arbeidet har vi implementert modellen for hastighetsfluktuasjoner i FFIs egenutviklede endelig-volum Euler-Lagrange-løser for kompressibel strømning, som er basert på de volummidlede Navier-Stokes-ligningene. Modellen kan uttrykkes

$$\tilde{R} \approx \tilde{u}^2 \frac{C_{\text{sep}} \alpha_p}{\alpha - C_{\text{sep}} \alpha_p},$$

hvor $\tilde{R}$ er korrelasjonen av hastighetsfluktuasjoner, $\tilde{u}$ er middelhastigheten, og $\alpha_{\text{p}} = 1 - \alpha$, hvor α er volumfraksjonen av gass. Modellen har en parameter, C_{sep}, som vi estimerer med ABC-SMC-algoritmen, basert på resultatene fra en simulering av samme system hvor vi beregner strømningen i detalj rundt hver partikkel. Å bruke ABC-SMC-algoritmen for parameterestimering er en interessant framgangsmåte fordi den estimerte verdien er optimal for den spesifikke implementasjonen av strømningsløseren.

Avhengig av om vi bruker en tilnærmet luftmotstandsmodell eller partikkelkreftene fra de partikkel-oppløste simuleringene, blir parameteren estimert til å være henholdsvis $C_{\text{sep}} = 1,4$ og $C_{\text{sep}} = 1,6$. Den fysiske betydningen av disse verdiene er at det gjennomsnittlige volumet til den separerte strømningen bak hver partikkel er 1,4 eller 1,6 ganger større enn volumet til partikkelen. At den estimerte parameterverdien avhenger av valget av drag-lov betyr at for å få en fysisk betydningsfull verdi for C_{sep}, må vi anvende en drag-lov som nøyaktig representerer både de transiente og de kvasistødige kreftene på partiklene.

Contents

Preface

This report contains the results from a short study conducted as part of the 2019 summer internship at the FFI, where the first author has worked at FFI for two months under supervision of the second author.

Oslo, 17. June, 2020
Bernhard Nornes Lotsberg
Andreas Nygård Osnes

1 Introduction

Shock-wave particle cloud interaction is a multi-scale flow problem where particle-scale physical problems are dynamically important. Current models for high-speed dense particle-laden flows that are applicable to engineering-scale problems require models for particle-scale flow processes. In models based on the volume-averaged Navier-Stokes equations, the particle-scale flow processes appear in the equations as unclosed terms. Most models simply set these terms to zero, except for the terms related to particle drag. In shock-wave particle cloud interaction, neglection of these terms can lead to erroneous flow predictions, such as particle accumulation near the downstream cloud edge [11]. It is therefore important to develop accurate models for particle-scale flow processes, so that reliable engineering-scale computations can be performed.

Velocity fluctuation correlations in particular, are important for shock-wave particle cloud interaction. Previous studies have investigated these terms in both two-dimensional [3] and three-dimensional studies [4, 5, 6]. The velocity fluctuation correlations impose effective forces on the flow through their spatial gradients, and are therefore particularly important around the particle cloud edges. Flow dynamics in these regions, such as the generation of the reflected shock wave, can therefore be affected by velocity fluctuations. For shock-wave particle cloud interaction, the reflected shock wave is important because it determines the conditions of the flow that enters the particle cloud.

1.1 Goal

In this project, we will test a simple model for fluctuations made by particle wakes in shock particle interactions. The model was proposed in a recent study based on the results from particle-resolved simulations [5], and was shown to be reliable over a range of particle sizes and flow conditions [6]. In the current work, the model is implemented in an Eulerian-Lagrangian dispersed flow model, which does not resolve the flow around each particle. The goal is to see whether accounting for particle-scale velocity fluctuations, specifically the effect of particle wakes, improve the predictions by the Eulerian-Lagrangian model. We especially want to see if the addition of the velocity fluctuation model improves the prediction of the reflected shock, which the baseline Eulerian-Lagrangian model predicts to be significantly weaker than that observed in the particle-resolved simulations.

1.2 Motivation

The fluctuation model tested in this project could give us the ability to more accurately simulate engineering scale, three-dimensional systems with an Eulerian-Lagrangian dispersed flow model. However, the model quality needs to be tested against accurate reference data.

Ultimately, the system of interest is an explosively dispersed layer of particles, which features $O(10^9)$ particles. In this problem, the particle layer is initially compressed by the blast wave, before being diluted and transitioning through a stage where the particle volume fraction remains in the dense gas-solid flow regime for an extended period of time. It is this regime where the current dispersed flow model is applicable, and where existing dispersed flow models has difficulties in obtaining accurate flow predictions.

2 Governing equations and numerical method

2.1 Governing equations

For compressible flow in one dimension, the Navier-Stokes equations become

$$\partial_t \rho + \partial_x (\rho u) = 0, \tag{2.1}$$

$$\partial_t (\rho u) + \partial_x (\rho u u + p - \sigma) + F = 0, \tag{2.2}$$

$$\partial_t (\rho E) + \partial_x (\rho E u + p u) = \partial_x (\sigma u) - \partial_x (\lambda \partial_x T), \tag{2.3}$$

where ρ is the mass density, u is the flow velocity, p is the pressure, $\sigma = 4\mu\partial_x u/3$ is the viscous stress tensor, $E = e + u^2/2$ is the total energy per unit mass, where e is the internal energy per unit mass, λ is the heat conductivity, and T is the temperature. In the current study, we apply the ideal gas equation of state to relate pressure, density and internal energy, with an adiabatic index $\gamma = 1.4$. The viscosity is governed by the power-law $\mu = \mu_0 (T/T_0)^{0.76}$, and temperature is related to the internal energy by a constant heat capacity. The heat conductivity and viscosity are related by a constant Prandtl number of 0.7.

Resolving all relevant scales around each particle in an engineering-scale problem would be too computationally costly, therefore we will deal with the volume-averaged form of eqs. (2.1) to (2.3). (2.1). The volume averaged version of eq. (2.1) is

$$\partial_t \overline{\rho} + \partial_x (\overline{\rho u}) = 0, \tag{2.4}$$

where $\bar{\cdot}$ denotes a volume-averaged variable. We then define some new variables

$$\frac{\overline{\rho u}}{\overline{\rho}} = \tilde{u}, \tag{2.5}$$

$$\overline{\rho} = \alpha \langle \rho \rangle. \tag{2.6}$$

Here, $\overline{\rho}$ is the volume-averaged density, while $\langle \rho \rangle$ is the phase-averaged density. α is the gas volume fraction, and is related to the particle volume fraction, α_p, by $\alpha = 1 - \alpha_\mathrm{p}$. Equation (2.4) becomes

$$\partial_t (\alpha \langle \rho \rangle) + \partial_x (\alpha \langle \rho \rangle \tilde{u}) = 0. \tag{2.7}$$

Applying the same procedure to eqs. (2.2) and (2.3) (see [5]) yields

$$\partial_t (\alpha \langle \rho \rangle \tilde{u}) + \partial_x \left(\alpha \langle \rho \rangle \tilde{u}^2 + \alpha \langle p \rangle - \alpha \langle \sigma \rangle + \alpha \langle \rho \rangle \tilde{R} \right) = \frac{1}{V} \int_S p n dS - \frac{1}{V} \int_S \sigma n dS, \tag{2.8}$$

and

$$\begin{aligned} \partial_t \left(\alpha \langle \rho \rangle \tilde{E} \right) + \partial_x \left(\alpha \langle \rho \rangle \tilde{E} \tilde{u} + \alpha \langle p \rangle \tilde{u} \right) &= \partial_x (\alpha \langle \sigma \rangle \tilde{u}) - \partial_x (\alpha \langle \lambda \partial_x T \rangle) \\ -\partial_x (\alpha \langle \rho e'' u'' \rangle) - \partial_x \left(\alpha \langle \rho \rangle \tilde{R} \tilde{u} \right) &+ D^u + D^p + D^\mu + D^{ap} + D^{a\mu} \\ + \frac{1}{V} \int_S p u n dS - \frac{1}{V} \int_S \sigma u n dS &+ \frac{1}{V} \int_S (\lambda \partial_x T) n dS, . \end{aligned} \tag{2.9}$$

where $\tilde{R} = \widetilde{u'' u''}$ denotes the velocity fluctuation correlation, where $u'' = u - \tilde{u}$. The integral terms are caused by the presence of the particles, where S denotes the dispersed phase boundary, and n is the normal vector pointing into the gas phase. The terms labeled $D^{\cdot}$ are diffusive fluctuation correlation terms, whose definitions can be found in [5]. In the simulations conducted here, they are set to zero, since their importance in shock-wave particle cloud interaction has not been investigated, and no appropriate closures exists.

2.1.1 Fluctuation model

$\tilde{R}$ is a term describing the velocity fluctuation correlation. This is where the proposed

$$\tilde{R} \approx \tilde{u}^2 \frac{\alpha_{\text{sep}}}{\alpha - \alpha_{\text{sep}}} \tag{2.10}$$

is needed [6], where in the current work we take $\alpha_{\text{sep}} = C_{\text{sep}}\alpha_{\text{p}}$. The parameter C_{sep} is to be determined with the aid of results from particle resolved, three dimensional simulations of a similar system.

2.1.2 Drag laws

The drag law we have chosen for our baseline solver is expressed

$$C_{\text{d}} = \frac{24}{Re_{\text{p}}}\left(1 + 0.15Re_{\text{p}}^{0.687} + 0.0175\left(1 + 4.25 \times 10^4 Re_{\text{p}}^{-1.16}\right)^{-1}\right), \tag{2.11}$$

([10], originally from Clift and Gauvin [1]). Here, $Re_{\text{p}} = \rho u D_{\text{p}}/\mu$, where D_{p} is the particle diameter.

In addition, we want to see whether the choice of drag model affects the estimated fluctuation constant C_{sep}. To do this, we will use saved force values from the particle-resolved simulation, and interpolate these. This should give drastically more accurate values for drag forces, and possibly give us a different C_{sep}. Also, we should then be able to determine the impact of a good fluctuation model versus a good drag model. In order to avoid unphysical effects such as particles imposing a force on the gas before there is any relative velocity between the particle and the gas, our interpolated drag function $f(x,t)$ will return zero until a shock is detected at each particle.

An alternative drag law we also want to use is the one from Parmar [9]. The expression for the drag-coefficient in Parmar's drag law is rather lengthy, and will therefore not be stated here. An advantage in this law over the one described in eq. (2.11), is that it is a function of the Mach number as well as the Reynolds number.

2.2 Numerical method

To numerically solve (2.7) - (2.9), we use an in-house finite volume Eulerian-Lagrangian code. Two separate flux schemes are used in this study: A Lax-Friedrich scheme, and the HLLC Riemann solver [12] which has been modified to solve the volume averaged equations, as in [7]. In both cases, we apply first-order reconstruction of primitive variables to the control volume faces. A third order Runge-Kutta scheme is used to advance the solution in time.

The particles are treated as point particles, using an approximate drag law to calculate drag force. Note that particle-volume is accounted for in the continuous phase equations. To match the particle-resolved simulations, the particles are locked in place. However, at each step, the particle velocity is advanced with a backward Euler scheme, while position is advanced with a Crank-Nicholson scheme, before being reset to their initial values. The change in particle momentum before the reset, which is related to the drag law, defines the force imposed on the fluid phase, F, c.f. eq. (2.2).

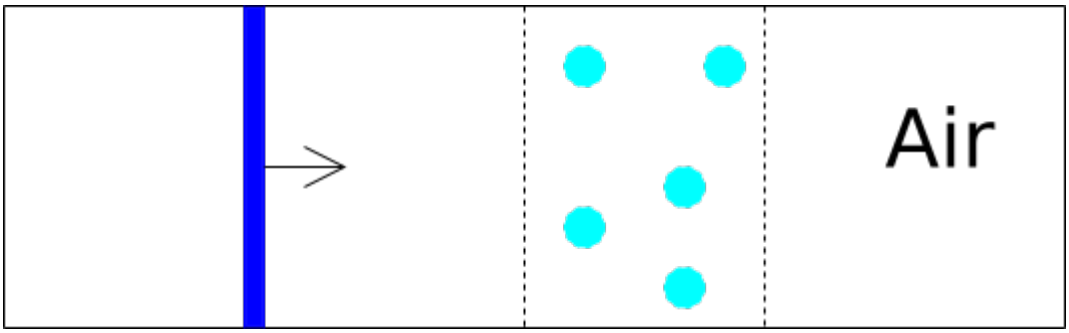

Figure 2.1 Illustration of the system under investigation in the study. The Mach 2.6 shock wave starts $0.1L$ *upstream of the particle cloud, and propagates from the left to the right. The particle cloud, with a particle volume fraction of* $\alpha_p = 0.1$ *is located between* $0 \leq x \leq L$.

2.3 Data

The particle resolved data [6] is an ensemble-averaged dataset of ten separate particle-resolved simulations, each having the same α, but different positions of the particles. This is to reduce noise caused by fluctuating α caused by a low number of particles.

2.4 Initial conditions

As seen in figure 2.1, our initial system contains air with a shock wave moving towards a gas containing particles. These initial conditions are statistically equal to the particle resolved data used for comparison. The particle cloud has statistically planar upstream and downstream cloud edges. The incident shock wave has a Mach number, $M = 2.6$, and propagates into air at atmospheric conditions. The atmospheric conditions are

$$\rho_{\text{atm}} = 1.2048 \text{ kg/m}^3, \quad u_{\text{atm}} = 0 \text{ m/s}, \quad p_{\text{atm}} = 101.325 \text{ kPa}, \tag{2.12}$$

resulting in the post-shock conditions

$$\rho_{\text{shock}} = 4.1553 \text{ kg/m}^3, \quad u_{\text{shock}} = 633.48 \text{ m/s}, \quad p_{\text{shock}} = 782.23 \text{ kPa}. \tag{2.13}$$

The heat capacity ratio is set so that $T_{\text{atm}} = 298$ K, and the viscosity is $\mu_{\text{atm}} = 1.8 \times 10^{-5}$ kg/(ms).

The particle layer, consisting of particles with diameter $D_{\text{p}} = 4^{-1/3} \times 10^{-4}$ m, is located between $0 \leq x \leq L$, where $L = 3 \cdot 4^{5/3} \, D_{\text{p}}$.

The total number of control-volumes used in each simulation of this study is 174. This corresponds exactly to the number of averaging volumes used to process the particle-resolved data, and their locations and boundaries are also matched. The control-volume widths and heights are set so that the entire set of particles occupy a volume fraction of 0.1 within $0 \leq x \leq L$.

2.5 The ABC-SMC algorithm

We use the ABC-SMC (Approximate Bayesian Computation - Sequential Monte Carlo) algorithm [2] to calculate the best fitting value for C_{sep}. The algorithm is as follows (with a few modifications, written in bold):

1. **Set starting tolerance $\epsilon_0 = \infty$ (or any large number).**
2. Define how many iterations should be calculated T.
3. For t $\in [0, T]$ (This could be a while loop, but we wish to avoid potential infinite looping.)
4. $i = 1$
5. while $i < N + 1$ (N being the number of samples per t).
6. If $t = 1$: Sample candidate parameter $\tilde{C}$ from the prior $\pi(C^0)$
7. Else: Sample C_{sample} from C^{t-1} with weights ω^{t-1}.
8. Perturb C_{sample} via the perturbation kernel K_t, so that: $\tilde{C} = C_{\text{sample}} + K_t(\cdot|\tilde{C})$
9. Run simulation using candidate $\tilde{C}$, getting solution y_{sim}
10. Calculate error $\Delta(y_{\text{sim}}, y_{\text{actual}}) = \frac{(u_{\text{sim}}-u_{\text{actual}})^2}{u_{\text{actual}}^2} + \frac{(p_{\text{sim}}-p_{\text{actual}})^2}{p_{\text{actual}}^2} + \frac{(\rho_{\text{sim}}-\rho_{\text{actual}})^2}{\rho_{\text{actual}}^2}$
11. If $\Delta(y_{\text{sim}}, y_{\text{actual}}) < \epsilon$:
12. $i \leftarrow i + 1$
13. $C_i^t = \tilde{C}$
14. else:
15. return to line 5
16. **Reduce ϵ to a percentile of the candidate errors.**
17. if $t = 1$
18. $\omega_i^1 = 1$
19. else
20. $\omega_i^t = \frac{\pi(C_i^t)}{\sum_{j=i}^N \omega_i^{t-1} K_t(C_i^t | C_j^{t-1})}$ (Importance sampling)
21. Normalize ω_i^t

where subscript "actual" refers to the results of the particle-resolved simulations. In our implementation, each step of the loop in step 5 is run in parallell, meaning for each step t, we have N instances of the while-loop running (we have chosen to run one sample per thread), only finishing when the criteria in step 11 is met. We use a Gaussian perturbation kernel, with variance $\sigma^t = 2\text{Var}(C^t)$ [2]. The prior $\pi(C)$ is a known distribution describing all we already know about the parameter C_{sep} before calculating anything. We have defined our prior as

$$\pi(C) = \begin{matrix} \frac{1}{10}, & C \in [0, 10] \\ 0, & C \notin [0, 10] \end{matrix} . \tag{2.14}$$

C^t is the parameter the algorithm is estimating at the t'th iteration of the algorithm.

The reason we have chosen to reduce the tolerance by percentiles, which is a rather different method than statically pre-defining the tolerances and looping over them, which is the usual way to implement ABC-SMC, is that we do not know what tolerances make sense for our system. Starting with a very large tolerance and then reducing it by percentiles is a very general method that does not require any knowledge about the size of the errors. For the problem in this study, this approach converges quickly, and even more rapid convergence is obtained with the aid of a reasonable prior.

3 Results

This section presents the results of the numerical simulations. First, results from the baseline solver with direct application of the fluctuation model, with $C_{\text{sep}} = 1.17$ as found at late time in the particle-resolved simulations, are presented. Next, we apply the ABC-SMC algorithm to estimate the best value of C_{sep}, and present the simulation results based on the new value of C_{sep}. Finally, the sensitivity with respect to the drag-law is shown. Figures 3.1 to 3.3 have common labels, which refer to the models as described in table 3.1. Time is normalized using a time-scale

$$t_0 = 2.9L/U_{\text{s}}, \tag{3.1}$$

where U_{s} is the shock wave velocity, which is the time it takes for the shock wave to travel a distance equal to the domain length.

3.1 Directly derived C_{sep}

The value $C_{\text{sep}} = 1.17$, corresponding the value of α_{sep} at late time in the simulations of [6], yields the results shown in figs. 3.1 to 3.3. The pressure at late time, shown in fig. 3.1 differs significantly from the results of the particle-resolved simulations, which for the purpose of this study are considered the correct solution. The reflected shock wave is much weaker in the baseline solver, yielding too low pressures and too high velocities upstream of and within the particle layer. This is the case both with the application of the Lax-Friedrich type solver and the HLLC solver. The inclusion of $\tilde{R}$ in the momentum equation has a significant impact on the flow solution, generating a stronger reflected shock as well as a stronger expansion region around the downstream cloud edge. Especially for the Lax-Friedrich solver, this is an important difference, because the baseline version does not display any overexpansion. For the HLLC solver, the addition of the fluctuation model leads to numerical artifacts within the cloud, displaying strong spikes throughout the cloud. Similar observations can be made for the velocity field, shown in fig. 3.2.

In fig. 3.3, the velocity fluctuations are compared against the particle-resolved data at late time. At this point, both the LF and HLLC solvers overpredict the fluctuations within the cloud, but the agreement of the profiles with the particle-resolved data is quite good. Notably, the particle-resolved data display a non-negligible magnitude of the fluctuations downstream of the cloud edge, which is not captured by the model. This is expected and in accordance with the derivation of the model, because the model is only intended to represent particle wakes, which are not present in regions without particles.

Table 3.1 Description of the models referred to by the legends in figures figs. 3.1 to 3.3

Label	Description
"1D"	Current simulations
"3D"	Three dimensional, particle-resolved simulation
"only rhou fix"	$\tilde{R}$ is only applied in the momentum equation (2.8)
"no pressure"	$\tilde{R}$ is applied in momentum equation and energy equation (2.9), but not corrected for in pressure
"full model"	$\tilde{R}$ is applied everywhere relevant

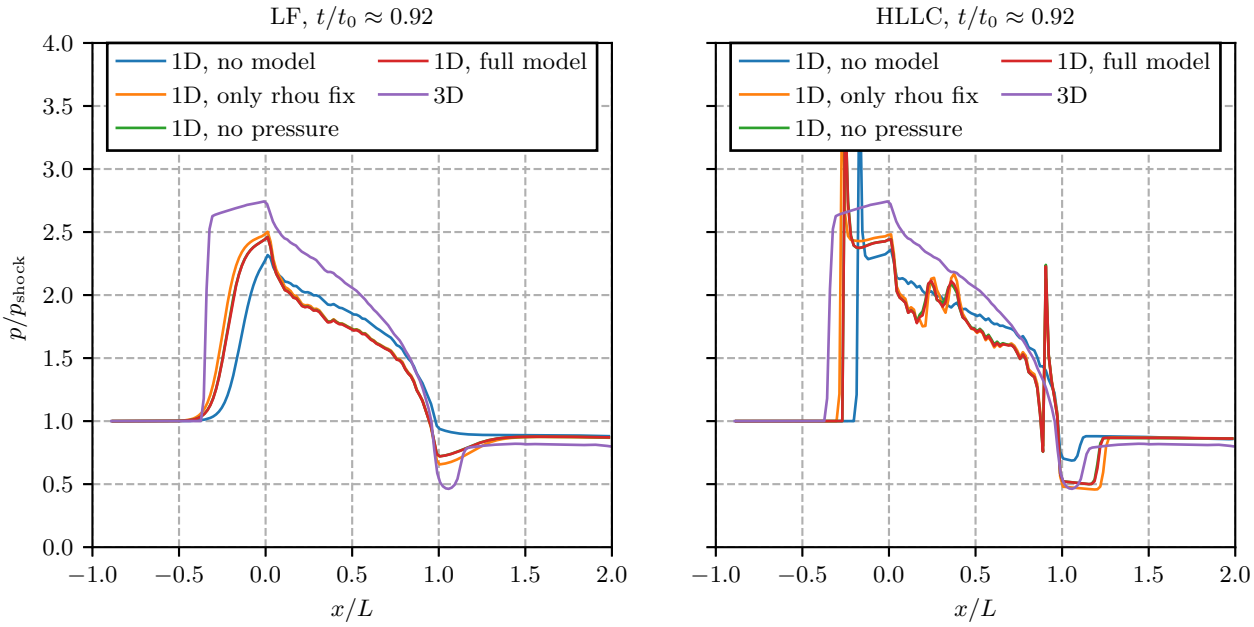

Figure 3.1 *The pressure p, solved using both LF (left) and HLLC (right) with varying degrees of corrections applied.*

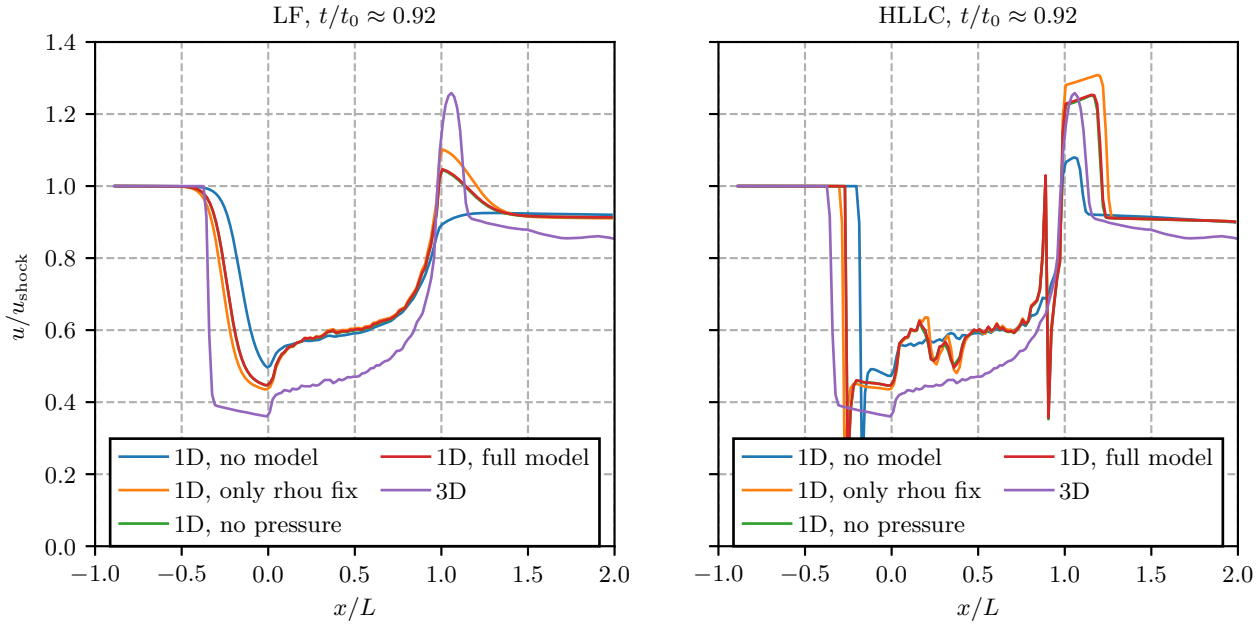

Figure 3.2 *The flow velocity, ũ, solved using both LF (left) and HLLC (right) with varying degrees of corrections applied.*

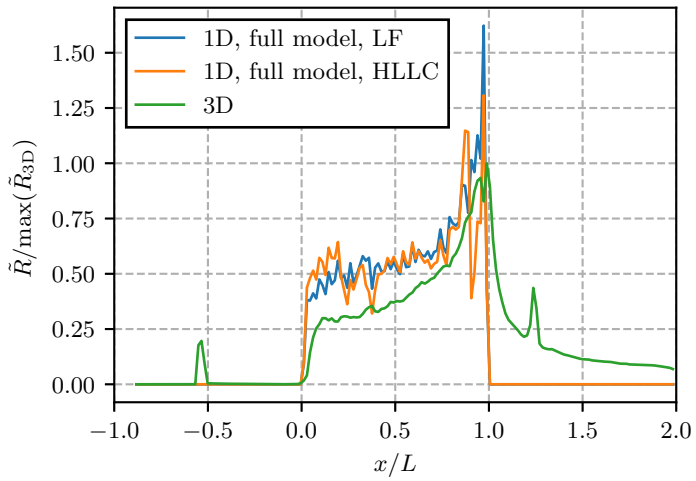

Figure 3.3 Velocity fluctuation correlation model, $\tilde{R}$, solved using both LF and HLLC, and the velocity fluctuation correlation form the particle-resolved data at $t/t_0 \approx 0.92$.

3.2 Statistically derived C_{sep}

The results in figs. 3.1 and 3.3 are obtained with $C_{\text{sep}} = 1.17$, which is the value obtained at a single, late, time-point in the particle-resolved simulations. A more robust estimate can be obtained by optimizing the value of C_{sep} by comparison of the dispersed flow model against the particle-resolved data. In order to do this, we apply the ABC-SMC method. Figure 3.4 shows the estimated distribution of C_{sep} with increasing number of iterations of the ABC-SMC algorithm. The distribution converges towards the value $C_{\text{sep}} = 1.4$.

Figure 3.5 shows the velocity and pressure at late time from the flow solver with this value of C_{sep} as well as those obtained with $C_{\text{sep}} = 1.17$. There appears to be only a minor difference between these values of C_{sep}, indicating that the model is not very sensitive to the exact value of C_{sep} in the range $1.17 - 1.4$. However, the change from $0 - 1.17$ has important consequences for the flow, as discussed above.

3.3 Drag law comparisons

The drag-law is a central part of the Eulerian-Lagrangian dispersed flow model, and it is therefore of interest to compare the results obtained with different models for particle drag. Figure 3.6 compares the flow velocities of the particle-resolved simulations with the one-dimensional solutions using the drag-law of Clift and Gauvin, eq. (2.11), as well as the model of [9], here referred to as the Parmar drag-law. In addition, we use the particle-forces from the particle-resolved simulations directly, and consider this to be our best possible model for particle-drag.

Note that the value of C_{sep} is estimated to different values with the ABC-SMC algorithm, depending on the drag law. When we apply the forces from the particle-resolved simulations, the estimated C_{sep} is 1.6 as opposed to 1.4 for the Clift and Gauvin drag law. C_{sep} has not been estimated when using the Parmar drag-law due to time constraints. In comparing the different drag-laws, we apply a single value of $C_{\text{sep}} = 1.5$, which is in the middle of the interval identified from the C_{sep} estimates mentioned. The reason for using this value with all the drag laws is that the effect of the

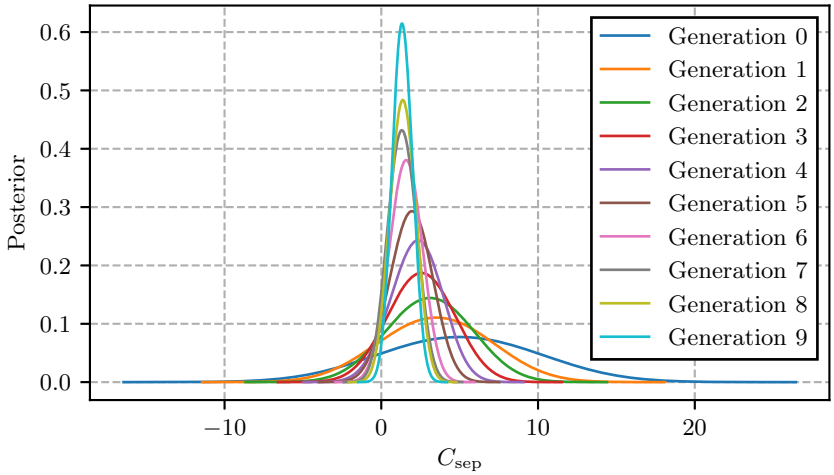

Figure 3.4 Statistical distribution of C_{sep} using the drag law of Clift and Gauvin.

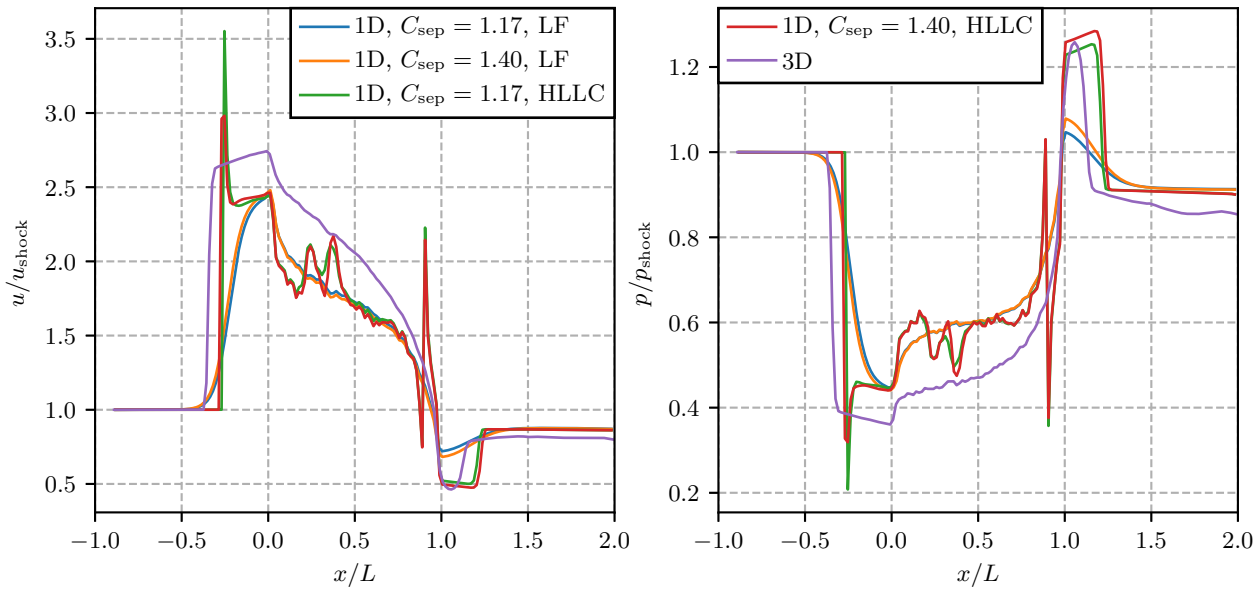

Figure 3.5 The velocity (left) and pressure (right), solved using both LF and HLLC with two different values of C_{sep}. The line colors are the same in both plots, and therefore the legend has been split to avoid overlapping the lines.

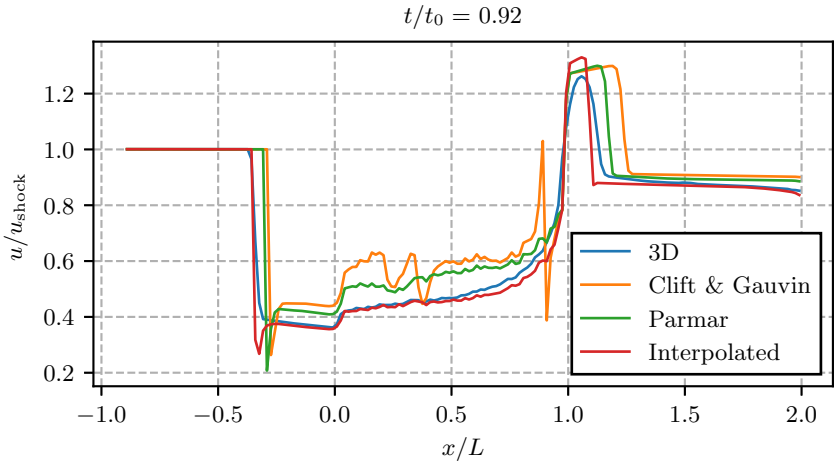

Figure 3.6 Flow velocities in the particle-resolved simulations and in the current one-dimensional simulations, with the drag-law of Clift and Gauvin, as well as the drag-law by Parmar [9]. Also shown are the results where the particle forces from the particle-resolved simulations are applied directly in the one-dimensional simulations. For these simulations, the value $C_{\text{sep}} = 1.5$ has been used.

drag law can be isolated. Additionally, all one-dimensional simulations shown in fig. 3.6 use the HLLC Riemann solver.

The results show that the Parmar drag-law is a considerable improvement over the drag-law of Clift and Gauvin. Using the Parmar drag-law results in a stronger reflected shock, stronger shock-wave attenuation and a slightly stronger overexpansion. These changes bring the solution closer to the results from the particle-resolved simulations. Incidentally, the large spike near the downstream cloud edge obtained with the Clift and Gauvin drag-law is not present with Parmar's drag-law. However, applying the drag from the particle-resolved simulations is yet another significant improvement over using Parmar's drag law. This is possibly due to the strong initial transient following shock-wave impact on each particle. The particle-drag is significantly higher during the initial interaction with the shock wave than in the later stages where quasi-steady drag is the dominant contribution to particle-drag.

4 Discussion

4.1 Validity of model

The statistical analysis gives a nonzero C_{sep}, meaning the system is more accurate with the fluctuation model than without it. One concern here is that the best value differs depending on how the drag forces are calculated, with there being a 0.2 difference between the value obtained with the Clift and Gauvin drag law and the value obtained with drag forces interpolated from the particle-resolved data. This probably means that the fluctuation model is being fitted to compensate somewhat for the errors from estimation of particle drag. This additional compensation is a confounding factor when it comes to estimating the quality of the velocity fluctuation model. The estimated value of C_{sep} is however nearly invariant of the flux-scheme, which is encouraging.

4.2 Quality of our ABC-SMC implementation

The way we define our error could influence what result ABC-SMC gives. In addition, the way we chose to define the standard deviation in the Gaussian perturbation has an effect on the results. If we were to change the standard deviation, the final distribution would look different. Therefore it is important to remember that fig. 3.4 may not necessarily be the most "correct" posterior distribution. We are however, only interested in the most likely value, which is easily extracted from these distributions.

4.3 Further improvement

The next logical step to improve this fluctuation model is to make it depend on time. In reality, a wake takes a bit of time to manifest fully. This should ideally be represented in the model via some gradual increase before the full effect is present. In addition, the current simulation has locked the particles in place, in order to compare against the particle-resolved simulations. An interesting next step is therefore to investigate how the model affects the results if the particles are allowed to move.

Including a model for the transient forces during shock-particle interaction is a natural extension of the current work. A potential model for this interaction can be found in [8].

The ABC-SMC algorithm we used could be improved. Our parallelization scales linearly, but each t-step has to wait for all samples to be accepted, meaning the thread taking the longest time will hinder all the others. A way to improve this would be to have every thread sample new values until there are enough samples, then stopping them all. This would reduce the impact of one thread taking a lot of time.

4.4 Importance

The addition of the velocity fluctuation model has a significant effect on the results from the Eulerian-Lagrangian simulations. The improvement is comparable to that obtained going from the Clift and Gauvin drag-law to the drag-law of Parmar. However, even more sophisticated drag-laws has the potential to bring the results even closer to the particle-resolved results, as we have demonstrated by using the particle-forces from the particle resolved simulations directly.

5 Conclusions

Including the model for velocity fluctuations improves the quality of the Eulerian-Lagrangian simulations of shock-wave particle cloud interaction. However, further improvements are needed before we can expect to run an Eulerian-Lagrangian simulation of shock-wave particle cloud interaction and be confident that the results are representative of the real behavior of such systems. The current results indicate that improving models for drag has a strong effect on the results, and is therefore important. The initial transient following shock-wave impact on each particle is likely important for the generation of the reflected shock, and therefore the flow state within the entire particle cloud.

C_{sep} was estimated to 1.4 and 1.6, depending on the choice of drag-law. This has the physical interpretation that the volume of the separated flow behind each particle is 1.4 or 1.6 times larger than the volume of the particle. The volume of these separation regions can potentially be estimated from the particle-resolved data directly, and this can serve as an additional test for the fluctuation model.

References

[1] R. Clift and W. H. Gauvin. Motion of particles in turbulent gas streams. *Proc. Chemchea*, pages 14–28, 1970.

[2] Sarah Filippi, Chris P Barnes, Julien Cornebise, and Michael Stumpf. On optimality of kernels for approximate Bayesian computation using sequential Monte Carlo. *Statistical applications in genetics and molecular biology*, 12:1–21, 03 2013.

[3] Zahra Hosseinzadeh-Nik, Shankar Subramaniam, and Jonathan D. Regele. Investigation and quantification of flow unsteadiness in shock-particle cloud interaction. *International Journal of Multiphase Flow*, 101:186–201, 2018.

[4] Y. Mehta, T. L. Jackson, and S. Balachandar. Pseudo-turbulence in inviscid simulations of shock interacting with a bed of randomly distributed particles. *Shock Waves*, 0(0):0, 2019.

[5] Andreas Nygård Osnes, Magnus Vartdal, Marianne Gjestvold Omang, and Bjørn Anders Pettersson Reif. Computational analysis of shock-induced flow through stationary particle clouds. *International Journal of Multiphase Flow*, 114:268–286, 2019.

[6] Andreas Nygård Osnes, Magnus Vartdal, Marianne Gjestvold Omang, and Bjørn Anders Pettersson Reif. Particle-resolved simulations of shock-induced flow through particle clouds at different reynolds numbers. *arXiv preprint arXiv:1906.08299*, 2019.

[7] Andreas Nygård Osnes, Magnus Vartdal, and B. A. P. Reif. Numerical simulation of particle jet formation induced by shock wave acceleration in a Hele-Shaw cell. *Shock Waves*, 28(3):451–461, 2018.

[8] M. Parmar, A. Haselbacher, and S. Balachandar. Modeling of the unsteady force for shock–particle interaction. *Shock Waves*, 19(4):317–329, 2009.

[9] M. Parmar, A. Haselbacher, and S. Balachandar. Improved drag correlation for spheres and application to shock-tube experiments. *Aiaa Journal*, 48(6):1273–1276, 2010.

[10] J. D. Schwarzkopf, M. Sommerfeld, C. T. Crowe, and Y. Tsuji. *Multiphase flows with droplets and particles*. CRC press, 2011.

[11] T. G. Theofanous and C-H. Chang. The dynamics of dense particle clouds subjected to shock waves. Part 2. Modeling/numerical issues and the way forward. *International Journal Multiphase Flow*, 89:177–206, 2017.

[12] E. F. Toro. *Riemann solvers and numerical methods for fluid dynamics: a practical introduction*. Springer Science & Business Media, 2013.

About FFI

The Norwegian Defence Research Establishment (FFI) was founded 11th of April 1946. It is organised as an administrative agency subordinate to the Ministry of Defence.

FFI's MISSION

FFI is the prime institution responsible for defence related research in Norway. Its principal mission is to carry out research and development to meet the requirements of the Armed Forces. FFI has the role of chief adviser to the political and military leadership. In particular, the institute shall focus on aspects of the development in science and technology that can influence our security policy or defence planning.

FFI's VISION

FFI turns knowledge and ideas into an efficient defence.

FFI's CHARACTERISTICS

Creative, daring, broad-minded and responsible.

Om FFI

Forsvarets forskningsinstitutt ble etablert 11. april 1946. Instituttet er organisert som et forvaltningsorgan med særskilte fullmakter underlagt Forsvarsdepartementet.

FFIs FORMÅL

Forsvarets forskningsinstitutt er Forsvarets sentrale forskningsinstitusjon og har som formål å drive forskning og utvikling for Forsvarets behov. Videre er FFI rådgiver overfor Forsvarets strategiske ledelse. Spesielt skal instituttet følge opp trekk ved vitenskapelig og militærteknisk utvikling som kan påvirke forutsetningene for sikkerhetspolitikken eller forsvarsplanleggingen.

FFIs VISJON

FFI gjør kunnskap og ideer til et effektivt forsvar.

FFIs VERDIER

Skapende, drivende, vidsynt og ansvarlig.

FFI's organisation

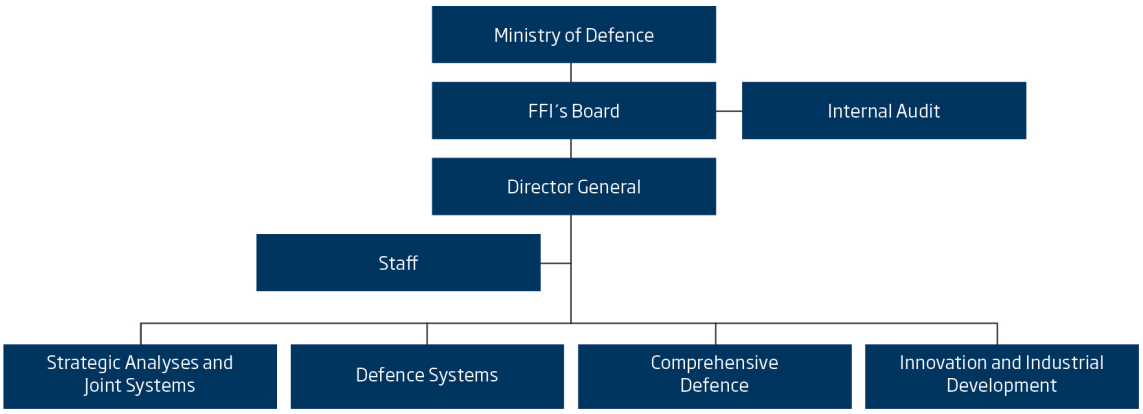

Forsvarets forskningsinstitutt
Postboks 25
2027 Kjeller

Besøksadresse:
Instituttveien 20
2007 Kjeller

Telefon: 63 80 70 00
Telefaks: 63 80 71 15
Epost: ffi@ffi.no

Norwegian Defence Research Establishment (FFI)
P.O. Box 25
NO-2027 Kjeller

Office address:
Instituttveien 20
N-2007 Kjeller

Telephone: +47 63 80 70 00
Telefax: +47 63 80 71 15
Email: ffi@ffi.no

FFI Forsvarets forskningsinstitutt
Norwegian Defence Research Establishment